THE ASTROPHYSICAL JOURNAL, 436:848–858; 1994 December 1

QUIESCENT ACCRETION DISKS IN BLACK HOLE X-RAY NOVAE[1]

JEROME A. OROSZ[2] AND CHARLES D. BAILYN[2,3,4]
Department of Astronomy, Yale University, P.O. Box 208101, New Haven, CT 06511-8101; orosz@astro.yale.edu, bailyn@astro.yale.edu
RONALD A. REMILLARD[3]
Center for Space Research, Massachusetts Institute of Technology, Cambridge, MA 02139; rr@space.mit.edu
JEFFREY E. MCCLINTOCK[3]
Harvard-Smithsonian Center for Astrophysics, 60 Garden Street, Cambridge, MA 02138; jem@cfa.harvard.edu
AND
CRAIG B. FOLTZ
Multiple Mirror Telescope Observatory, Tucson, AZ 85721; cfoltz@as.arizona.edu
Received 1994 March 7; accepted 1994 June 6

ABSTRACT

We present detailed time-resolved spectroscopy of the Balmer emission lines from two black hole binary systems in quiescence, A0620−00 and Nova Muscae 1991. We find extraordinary similarities between the two systems. There are 30–40 km s^{-1} velocity variations of the emission lines over the orbital period, the phases of which are not aligned with the expected phase of the motion of the compact primary. Detailed modeling of both systems is complicated by variable hot spot components, regions of optical thickness, and intermittent excess emission in the blue line wings of the Hα lines. Both sources also display low velocities at the outer edge of the accretion disk, implying a large primary Roche lobe and extreme mass ratios. These complications suggest that although simple optically thin, Keplerian α-disk models provide a useful parameterization of emission lines from these systems, the straightforward physical models they imply should be treated with great caution.

Subject headings: accretion, accretion disks — binaries: spectroscopic — black hole physics — stars: individual (A0620−00, Nova Muscae 1991) — X-rays: stars

1. INTRODUCTION

X-ray novae provide the clearest evidence for the existence of black holes in nature. In quiescence, the absorption line spectrum from the secondary star can be observed, and an orbital velocity curve constructed. From this, the mass function of the primary can be determined. In three cases (A0620−00: McClintock & Remillard 1986; Nova Muscae 1991: Remillard, McClintock, & Bailyn 1992; V404 Cyg: Casares, Charles, & Naylor 1992) $f(M) \gtrsim 3\ M_\odot$. In these cases, the primary is thus more massive than the most massive stable neutron star for any reasonable neutron star equation of state (Rhoades & Ruffini 1974; Chitre & Hartle 1976; Shapiro & Teukolsky 1983). Since the primary must be a compact object to produce the strong X-ray flux seen during the outburst, the only conclusion possible in the context of current physical and astrophysical theory is that the primaries in these three systems must be black holes.

It is thus of some interest to constrain the orbital parameters and physical conditions in these systems. The complex structure of the Balmer emission lines in quiescence offers a potential gold mine of information. Since these lines presumably originate in the accretion disk, they can be used both to examine the structure of the disk and to trace the motion of the primary star. Detailed studies of the Hα emission line of A0620−00 have been carried out by a number of authors (Johnston, Kulkarni, & Oke 1989, hereafter JKO89; Haswell & Shafter 1990, hereafter HS90; Marsh, Robinson, & Wood 1994, hereafter MRW94). Here we present data from Nova Muscae 1991 (=GR/GRS 1124−683, GU Mus), and also new high-quality data for A0620−00. Our analysis demonstrates great similarities between the two sources, reinforcing the similarities previously noted in the high-energy outburst behavior (Kitamoto et al. 1992; Della Valle, Jarvis, & West 1991), orbital parameters (Bailyn 1992; Remillard et al. 1992), and secondary star spectrum (Remillard et al. 1992). We find, however, that straightforward physical models of these data may be misleading.

2. OBSERVATIONS AND REDUCTIONS

Our initial spectral observations of Nova Muscae obtained 1992 April 3 (UT) are described by Remillard et al. (1992). Additional observations of Nova Muscae were carried out 1993 February 26/27–27/28 (UT) with the CTIO 4 m equipped with the RC spectrograph and a Tek1024 (1024 × 1024) CCD detector. The slit was rotated several times each night to maintain approximate alignment with the parallactic angle (Filippenko 1982). See Table 1 for the journal of observations. The phase coverage for the 1992 run is nearly complete and the phase coverage on each night in the 1993 run is about 80% complete. In addition to the spectra of Nova Muscae, we also obtained the spectra of several radial velocity standards with spectral types ranging from late G to late K, including lumi-

[1] Some of the data reported here were obtained at the Multiple Mirror Telescope Observatory, a joint facility of the Smithsonian Institution and the University of Arizona.
[2] Visiting Astronomer, Kitt Peak National Observatory, NOAO, operated by the Association of Universities for Research in Astronomy (AURA), Inc., under cooperative agreement with the National Science Foundation.
[3] Visiting Astronomer at Cerro Tololo Inter-American Observatory (CTIO), which is operated by the Association of Universities for Research in Astronomy (AURA), Inc., under contract with the National Science Foundation.
[4] National Young Investigator.

TABLE 1

JOURNAL OF OBSERVATIONS—NOVA MUSCAE

Date (UT) and Observatory	Number of Object Spectra	Exposure Time (minutes)	Seeing	Slit Width	Pixel Size (Å)
1992 Apr 2/3 CTIO[a]	21	20	~2".0	1".8–2".2	2.2
1993 Feb 26/27 CTIO (Night 1)	17	20	≲1.5	1.50	2.0
1993 Feb 27/28 CTIO (Night 2)	18	20	≲1.5	2.25	2.0

NOTE.—Spectra of flux and radial velocity standards were also taken on all nights.
[a] Complete phase coverage obtained.

TABLE 2

JOURNAL OF OBSERVATIONS—A0620−00

Date (UT) and Observatory	Number of Object Spectra	Exposure Time (minutes)	Seeing	Slit Width	Pixel Size (Å)
1991 Jan 11 MMT[a] (Night 1)	23	15	~1".0	1".25	0.8
1991 Feb 20 MMT (Night 2)	12	15	~3.0–5.0	1.25	0.8
1993 Dec 10 KPNO	2	15	≲1.5	1.50	1.7

NOTE.—Spectra of flux and radial velocity standards were also taken on all nights.
[a] Complete phase coverage obtained.

nosity classes V, III, and I. The spectra from a He-Ne-Ar lamp yielded wavelength calibrations with rms residuals typically ≲0.1 Å.

The initial spectral observations of A0620−00 were taken 1991 January 11 (UT) (Night 1) and 1991 February 20 (UT) (Night 2) at the Multiple Mirror Telescope. A TI 800 × 800 CCD detector was used along with a 1200 line per mm grating blazed at 5750 Å and a 1".25 × 180".0 entrance slit. See Table 2 for details. The A0620−00 spectra on Night 1 were collected over a period of slightly more than 7 hr, giving us almost complete phase coverage, while the Night 2 spectra were obtained over a period of only 4.5 hr. There were problems in subtracting a few of the night sky lines in the A0620−00 spectra because the TI CCD had poor vertical charge transfer efficiency (CTE), which affected the data along the dispersion axis of the CCD. The problem sky lines near Hα have the following wavelengths: $\lambda = 6297.0$ Å, 6363.4 Å, 6498.3 Å, 6562.5 Å and 6604.3 Å. These residual lines all have a similar appearance. They are certainly associated with sky subtraction problems because they appear in the sky spectra, their strength depends on the window extraction parameters, and they remain stationary over both observing nights. The sky removal problems make the data near the center of the Hα profiles useless, but fortunately the analysis presented below does not rely on that portion of the profile. Two additional spectra of A0620−00 were obtained 1993 December 10 (UT) with the Ritchey-Chrétien spectrograph attached to the Mayall 4 m telescope at Kitt Peak, using a 2048 × 2048 Tek CCD and the KPC-17B grating. See Table 2 for further details.

3. ANALYSIS OF PHASE-AVERAGED EMISSION LINES

We prepared "summed" emission-line profiles from our data sets by normalizing the spectra to their continua and averaging them (JKO89). Profiles were created for the 1992 Nova Muscae Hα data, the 1993 Nova Muscae Hα data (both nights), the 1993 Nova Muscae Hβ data (both nights), and the 1991 A0620−00 Hα data (both nights)—see Figure 1. The orbital phase coverage in all four cases is nearly complete, so the summed emission line profiles should show the phase-averaged behavior of the individual lines.

To model the emission-line profile from a circularly symmetric accretion disk, we assume the disk is flat, geometrically and optically thin, nonturbulent, and in Keplerian rotation (i.e., $V[R] \propto R^{-1/2}$). If the density function $f(r)$ of the emitting atoms (where the coordinate r is normalized to $r = 1$ at the outer edge of the disk) is a power-law expression of the form $f(r) = r^{-\alpha}$ (Shakura & Sunyaev 1973; Smak 1981; JKO89; Horne 1993), the emission-line profile, $F(u)$, can be written

$$F(u) \propto \int_{r_1}^{r_z} \frac{r^{3/2-\alpha}\, dr}{(1-u^2 r)^{1/2}}, \qquad (1)$$

where u is the dimensionless radial velocity ($u = 1$ when $r = 1$), r_1 is the ratio of the inner radius to the outer radius of the disk, and $r_z = \min(1, u^{-2})$ (Smak 1981). See Horne & Marsh

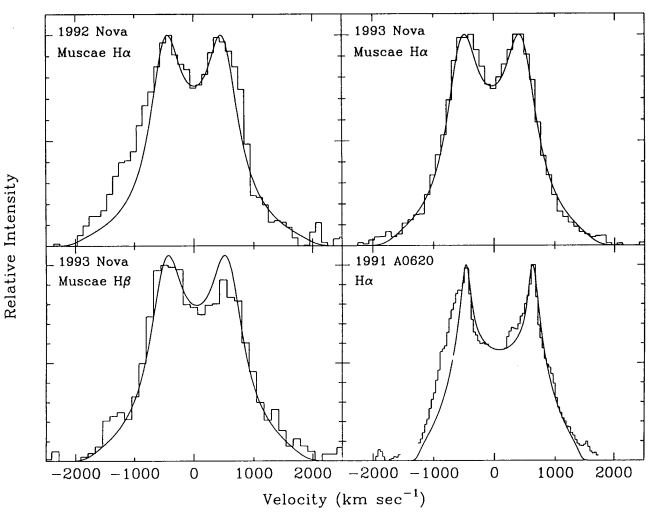

FIG. 1.—Four summed emission-line profiles are shown as histograms, and model fits (eq. [1]) are shown as solid lines. The x-axis scale has been put into velocity units, and the y-axis units are arbitrary with the continuum level at $y = 0$. Table 3 gives the model parameters. The gaps in the A0620−00 data near $v = -1400$, $v = 0$, and $v = 1800$ km s^{-1} indicate the regions where the sky subtraction problem affected the data.

TABLE 3

PARAMETERS FOR THE MODEL FITS TO THE SUMMED PROFILES SHOWN IN FIG. 1 AND OTHER PUBLISHED VALUES

Parameter	1992 Nova Muscae Hα	1993 Nova Muscae Hα[a]	1993 Nova Muscae Hβ[a]	1991 A0620−00 Hα[a]	JKO89 A0620−00 Hα
α	1.5	1.5	1.5	1.5	1.5
r_1	0.07 ± 0.01	0.07 ± 0.01	0.07 ± 0.01	0.15 ± 0.01	0.10
v_d (km s^{-1})	450 ± 10	450 ± 10	470 ± 15	550 ± 10	540 ± 15[b]

[a] Both nights of data are included in the summed profile.
[b] The disk velocity v_d and its error were found from a fit to phase-resolved profiles.

(1986a, b) and Smak (1981) for detailed discussions of this model.

3.1. *Model Parameters from Profile Fits*

Figure 1 shows the four summed profiles and the model fits described by equation (1). The best-fitting model parameters are given in Table 3. All four model fits shown in Figure 1 have $\alpha = 1.5$, as was found by JKO89 for A0620−00, and observed in other accretion disk systems (Filippenko et al. 1988; Horne 1993). However, MRW94 found $f(r) \propto r^{-1}$ for their A0620−00 data using a different technique. An interesting and unexpected result is that the Nova Muscae Hα line profile was asymmetric in the *line wings* in 1992, but not in 1993. The 1991 A06200−00 Hα profile is also asymmetric in the line wings in a similar manner to the 1992 Nova Muscae Hα profile. Such excess blue emission in A0620−00 was seen by HS90, but not by JKO89. Moreover, the 1993 A0620−00 Hα profile is symmetric in the line wings (Fig. 2). Thus both the asymmetry itself, and its transient nature, are common to Nova Muscae and to A0620−00. We will discuss this asymmetry in more detail in § 6.

3.2. *Disk Velocity at the Outer Edge and the Mass Ratio*

In principle, the binary mass ratio can be constrained by fitting the data to the model profiles and evaluating the projected velocity of the outer edge of the disk (JKO89). This analysis uses the separation of the peaks of the emission lines to set a lower bound on the size of the accretion disk, and hence the size of the primary Roche lobe which must contain it. By comparing the velocity of the outer edge of the disk to that of the secondary star, an upper limit on the mass ratio can be obtained. See JKO89 for a more detailed discussion of this method.

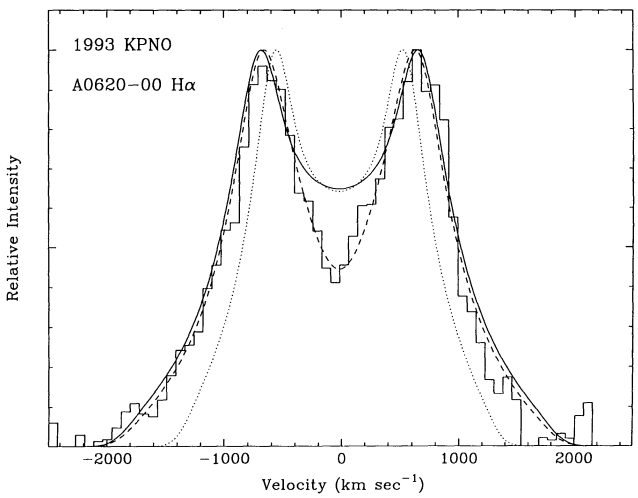

FIG. 2.—The A0620−00 Hα profile from 1993 December. Solid line is the model in the optically thin case (eq. [3]), and dashed line is the fit from the optically thick case (eq. [4]). Dotted line is the fit from the 1991 phase-averaged profile shown in Fig. 1. Clearly the peaks in the 1993 data have a larger separation than they did in 1991.

Since closed particle trajectories do not exist all the way out to the edge of the primary Roche lobe (e.g., Paczyński 1977), the maximum size of the disk is smaller than the primary Roche lobe. To quantify this limit, we have repeated and extended Paczyński's (1977) numerical experiments to find the largest possible closed streamline which is contained within the primary Roche lobe. Our calculations agree with those of Paczyński for the values of the mass ratios he considered, and we extended the calculations to more extreme mass ratios. With this information we can use our measured values of K_d/K_2 (defined as the ratio of the projected disk velocity to the semiamplitude of the secondary star's radial velocity curve) for Nova Muscae and A0620−00 to estimate the upper limits of the mass ratio q for both systems. The results of these calculations are given in Table 4. We note that the implied small mass ratios for Nova Muscae and A0620−00 in 1991 are in conflict with limits set by the observed ellipsoidal variations (Haswell et al. 1993; Antokhina & Cherepashchuk 1993).

This conflict between the mass ratios implied by the ellipsoidal variations and the velocity of the outer edge of the accretion disk (for the Nova Muscae data and the 1991 A0620−00 data) suggests that the assumptions behind one of these methods of constraining the mass ratio may be flawed. One obvious difficulty with the upper limit to q described here lies in the assumption that the disk is in Keplerian rotation at all radii. In fact, restricted three-body simulations show that the outer orbits are not circular. If the outermost parts of the disk deviate from Keplerian rotation, then the global emission-line profile could be changed significantly near the peaks, skewing the evaluation of the disk velocity v_d. Further numerical experiments are underway to determine whether non-Keplerian rotation can account for the anomalies in the implied mass ratio. The fact that the mass ratio implied by the 1993 A0620−00 Hα data is much larger may indicate that the

TABLE 4

UPPER LIMITS ON THE MASS RATIO DERIVED FROM THE DISK VELOCITY (§ 3.2)

Data Set	K_d/K_2 (km s^{-1})	Upper Limit on $q = M_2/M_1$
Nova Muscae: Hα (both years)	1.13 ± 0.020	0.0011
1991 A0620−00: Hα (both nights)	1.24 ± 0.023	0.0275
1993 A0620−00: Hα	1.47 ± 0.023	0.161

disk has contracted to a point where non-Keplerian motions are less important.

4. PHASE DEPENDENCE OF EMISSION LINES

To study the phase dependence of the disk, we binned the Hα data sets into six equal intervals in orbital phase. We adopt the phase convention used in JKO89, in which the maximum *blueshift* of the secondary star occurs at $\phi = 0.25$. Summed emission-line profiles at each phase were made from the data using the procedure described in § 3. The Hα profile for the 1993 A0620−00 data (where $\phi \approx 0.9$) is shown in Figure 2. The Hα profiles of the Nova Muscae and the 1991 A0620−00 data are shown in Figure 3. Unlike the profiles shown in Figure 1, these profiles in general have peaks of different heights, and the depth of the central minimum varies. The simple model described by equation (1) cannot account for either of these effects.

4.1. *Addition of a Hot Spot*

To calculate the models shown by solid lines in Figure 3, we relaxed the assumption of the axially symmetric disk. Following JKO89, we added the contribution of a simple hot spot to the power-law emissivity by defining the density function $f(r, \theta)$ as

$$f(r, \theta) \propto r^{-\alpha}[1 + \beta \sin(\psi_0 + \psi_{hs} - \theta)] , \quad (2)$$

where β is the amplitude of the hot spot, ψ_0 is the orbital phase of the observation, and ψ_{hs} is the (constant) phase of the hot spot with respect to the secondary star. For convenience, we define the variable $\psi = \psi_0 + \psi_{hs}$ to be the orbital phase of the hot spot (JKO89). The form described by equation (2) is simple and allows the expression for the emission-line profile $F(u)$ to be solved in closed form:

$$F(u) \propto \int_{r_1}^{r_z} \frac{r^{3/2-\alpha}\, dr}{(1 - u^2 r)^{1/2}} (1 - \beta u r^{1/2} \sin\psi) , \quad (3)$$

where u, r_1, and r_z have the same definition as in equation (1).

The parameters given in Table 5 were used for the model fits shown as solid lines in Figure 3. These values were determined by fixing the values of α and r_1 from Table 3, and varying β and ψ_{hs} until the best overall fit was found. From Figure 3, we see

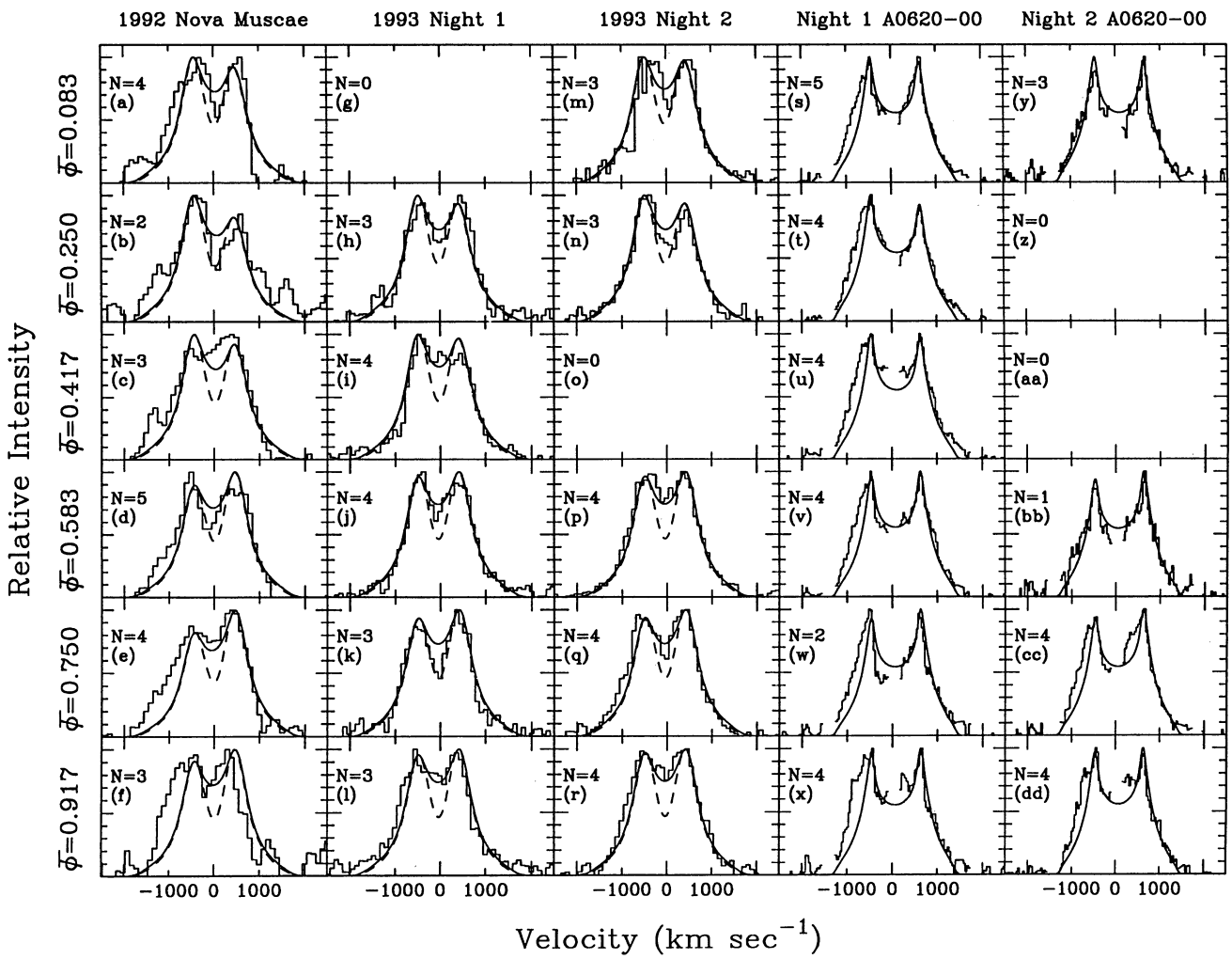

FIG. 3.—Phase-resolved Hα profiles for Nova Muscae and A0620−00 in 1991. The x-axis is in velocity units, and the y-axis units are arbitrary with the continuum level at $y = 0$. The orbital phase increases downward, with the average phase $\bar{\phi}$ indicated to the left. The number of spectra N that went into each average profile is indicated in each panel. Left-hand column is the 1992 Nova Muscae data, the next two columns show the data from the 1993 Nova Muscae run, and the two columns on the right show the data from the 1991 A0620−00 run. Solid lines were calculated using eq. (3) (optically thin case), and the dashed lines, shown with the Nova Muscae data only, were calculated using eq. (4) (the optically thick case). Table 5 gives the model parameters for the fits.

TABLE 5

PARAMETERS FOR THE MODEL FITS TO THE PHASE-RESOLVED PROFILES SHOWN IN FIGS. 2[a] AND 3[b] AND OTHER PUBLISHED VALUES

Parameter	1992 Nova Muscae Hα	1993 Nova Muscae Hα[c]	1991 A0620−00 Hα[c]	1993 A0620−00 Hα[d]	JKO89 A0620−00 Hα
α	1.5	1.5	1.5	1.5	1.5
r_1	0.07 ± 0.01	0.07 ± 0.01	0.15 ± 0.01	0.12 ± 0.01	0.09
β	0.15 ± 0.01	0.05 ± 0.01	0.05 ± 0.01	...	0.21
ψ_{hs} (degrees)	0 ± 5	0 ± 5	0 ± 5	...	7

[a] $i = 60°$ assumed in the optically *thick* case—*i* arbitrary for the optically *thin* case.
[b] $i = 70°$ assumed in the optically *thick* case—*i* arbitrary for the optically *thin* case.
[c] The fits include data from both nights.
[d] The disk velocity is $v_d = 650 \pm 10$ km s^{-1}.

that the observed height difference of the peaks is matched by the models for most of the profiles. Since the peak heights vary less in the 1993 Nova Muscae data and the 1991 A0620−00 data than they do in the 1992 Nova Muscae data, β is a factor of 3 greater for the 1992 Nova Muscae data than for the other data sets. The shape of the red line wings of most of the observed profiles is matched by the model profiles, while there is excess emission in the blue line wing at all phases in the 1992 Nova Muscae and 1991 A0620−00 profiles.

The shape of the hot spot described by equation (2) may not be a good physical representation of an actual hot spot (MRW94), since the hot spot intensity excess in equation (2) is present at all radii on the disk, whereas actual hot spots are thought to be confined to the outer parts of the disk. Also the angular width of the model hot spot is large, and actual hot spots may be more confined in their angular size (MRW94). We therefore considered a variety of alternative functional forms for the hot spot. In particular, we constrained the size of the hot spot in the radial direction by adding an inner cutoff radius, and the width of the hot spot in the angular direction by using different expressions for the hot spot. However, the new models with smaller hot spot area did not produce better fits than equation (3).

Since the heights of the two peaks differ only modestly, the value of β must be small. In the context of the spatially extended hot spots described by equation (2), this implies that the hot spot surface brightness is only moderately greater than the rest of the disk (on the order of 5%). Smaller hot spots with greater excesses are ruled out by the absence of a third sharp peak between the two main peaks (JKO89). Thus, in this case, the hot spot formalism of equation (2) appears to be justified.

4.2. *Optically Thick Lines*

Figure 3 demonstrates that the model described by equation (3) can predict the shape of the line wings and the heights of the peaks in most of the profiles shown. However, the depth of the central minima of the profiles is not well fitted, especially in the 1992 Nova Muscae data. Emission from optically *thick* regions can account for profiles with large central valleys (Horne & Marsh 1986a). Unlike the optically thin model profiles described by equations (1) and (3), the expression for the model line profile in the optically thick case has an explicit functional dependence on the inclination angle *i*. For small *i*, the central depression would appear less deep (Horne & Marsh 1986a). For A0620−00 and Nova Muscae, the inclination angle cannot be too small, since the photometric light curves of these systems show ellipsoidal variations indicative of moderate to high inclination angles.

By adapting the expressions of Horne & Marsh (1986a) into our formalism, the equation of the profile $F(u)$ in the optically thick case is given by the integral

$$F(u) \propto \int_{r_1}^{r_z} \frac{r^{3/2-\alpha}\,dr}{(1-u^2r)^{1/2}} (1 - \beta \sin \psi u r^{1/2}) \times [1 + 4\Upsilon^2(i)u^2r(1-u^2r)]^{1/2}\,, \quad (4)$$

where $\Upsilon(i) = \sin i \tan i$, u, r_1, and r_z have the same definition as in equation (1), and where we have used equation (2) for $f(r, \theta)$. This expression is valid for a completely optically thick disk. The main effect of the extra inclination-dependent term in equation (4) is to make the central minimum deeper than the depth calculated using equation (3), while the line wings calculated using equation (4) are almost identical to the line wings found using equation (3).

In Figure 3, model fits calculated using equation (4) are plotted with the dashed lines (shown with the Nova Muscae data only). The model parameters are the same as those listed in Table 5. The inclination angle used in the models for the optically thick case displayed in Figure 3 was $i = 70°$, a value within the approximate range of inclinations allowed by the ellipsoidal variations. No attempt was made to find a "best fit" value of *i*. In several panels of Figure 3 the optically thick models fit the data better than the optically thin models. It therefore seems likely that large regions of the disk may be optically thick, although the entire disk cannot be optically thick since many of the profiles have shallow central minima consistent with optically thin emission. Because the central depth of the profiles vary, we cannot constrain the inclination angle *i* by exploiting the functional dependence of the central depth on the inclination.

By looking along rows in Figure 3, we can compare profiles of similar orbital phase. An examination of the Nova Muscae data in the fifth row from the top (panels *e*, *k*, and *q*) shows that the depth of the central minimum varies with phase from year to year and even night to night. In contrast, the heights of the peaks in these three profiles are well predicted, so whatever controls the variable peak heights seems to stay more or less constant in phase. It may be that optically thick regions migrate around the disk, leaving the hot spot position unchanged. Differential rotation of structures in the disk may also contribute to the lack of phase constancy of these regions of optical thickness.

5. RADIAL VELOCITY VARIATIONS OF THE EMISSION LINES

The most straightforward way to find the mass ratio of a binary system is to measure the radial velocity curves of both

stars. In binary systems where the primary component is a compact object, radial velocity variations of emission lines from the accretion disk may trace the radial velocity variations of the primary. To search for Hα emission line radial velocity variations, we grouped the 1991 A0620−00 spectra and the 1993 Nova Muscae spectra slightly differently than was done for the profile analysis in § 4. Rather than group the spectra into equal size phase bins, we group them into phase bins of variable size, but with equal numbers of spectra in each bin.

5.1. *Measuring Velocities by Model Profile Fitting*

In § 4.1, we determined a function that has approximately the same shape as the emission line, namely the function described by equation (3). To find a value of the radial velocity for each profile, we computed a series of least-square fits by shifting the model profile center in one bin steps along wavelength. The radial velocity was then determined by fitting a parabolic function to the six points surrounding the minimum least-square value. The formal fitting error for the center of the parabola is taken as an estimate of the error. Typical errors found in this manner are in the range of 0.1–0.2 Å, or from about 5–10 km s^{-1}. We then fitted the derived velocities of the emission lines to a sinusoid, the amplitude of which should represent the velocity amplitude of the primary.

This technique is subject to several kinds of systematic errors. If the observed emission line profile is asymmetric, and the model used to fit it is symmetric, then the measured values of K_1 (the semiamplitude of the emission-line radial velocity curve) and γ (the systemic velocity) will be biased. However, we can choose model parameters so that the model profiles fit the data reasonably well, and we can inspect these fits using plots like Figure 3. Except for the systemic velocity γ, our results are not sensitive to small changes in the model parameters: values for γ obtained in this way are unreliable.

As shown in Figure 3, the phase-resolved A0620−00 profiles have excess emission in the blue line wings. As a result, emission-line radial velocity curves made including both peaks and both wings in the fitting region are likely to be biased. We therefore adjusted the starting bin of the fitting region to avoid the blue line wing and blue peak. Table 6 gives the sine curve parameters and the results are shown in Figure 4. The value of $K_1 = 32.6 \pm 2.7$ km s^{-1} found here is consistent with the value of $K_1 = 29 \pm 4$ km s^{-1} found by MRW94, who used a different technique. The phase zero point is surprisingly large ($\phi_0 = 0.12 \pm 0.013$, or about 43°). If the radial velocity variations of the emission lines accurately reflected the radial velocity variations of the primary, we would expect $\phi_0 = 0$. This phase shift cannot be caused by the excess blue emission because the blue line wing and blue peak were left out of the fitting region.

In order to demonstrate that the derived values of K_1 and ϕ_0 are insensitive to the model parameters, we performed the above fitting procedure with several sets of model parameters, which differ from those given in Table 5. In all cases the fitting region was the same as that shown in Figure 4. As long as we used only model parameters which give good fits to the profiles, the values of K_1 and ϕ_0 found from fitting the red wing and red peak were similar to the results quoted above.

We also used this method to find the emission-line radial velocity curve for the 1993 Nova Muscae Hα data. Since there is no excess blueshifted emission in the 1993 Nova Muscae data, we used the line wings and both peaks in the fitting region. However, we excluded five bins near zero velocity because the line core is in general not well fitted by the models (see Fig. 3). Table 6 lists the sine curve parameters for the Nova Muscae data, and Figure 5 shows the results. We find that

TABLE 6

BEST-FITTING SINE CURVE PARAMETERS FOUND FROM MODEL PROFILE FITTING (§ 5.1)

Parameter	1991 A0620−00 (Night 1)	1993 Nova Muscae (Both Nights)
Fitting region	Red wing and peak only	Both wings and both peaks
K_1 (km s^{-1})	32.6 ± 2.7	53.0 ± 7.4
ϕ_0	0.12 ± 0.013	0.10 ± 0.016
γ (km s^{-1})	78.3 ± 2.9	−53.8 ± 6.1

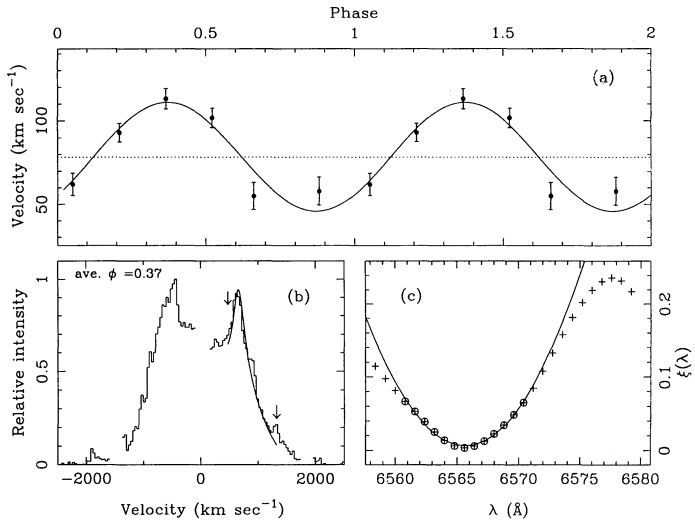

FIG. 4.—(*a*) The emission-line radial velocity curve for A0620−00, found from fitting model profiles to the line (§ 5.1, see Table 6 for the sine curve parameters). Each point is plotted twice for clarity. (*b*) The profile at $\phi = 0.37$. The edges of the fitting region are indicated by arrows. (*c*) The least-square fitting curve (referred to as $\xi[\lambda]$) shown with the crosses for the profile shown in (*b*). The circled crosses are the points used to fit the parabola (*solid line*).

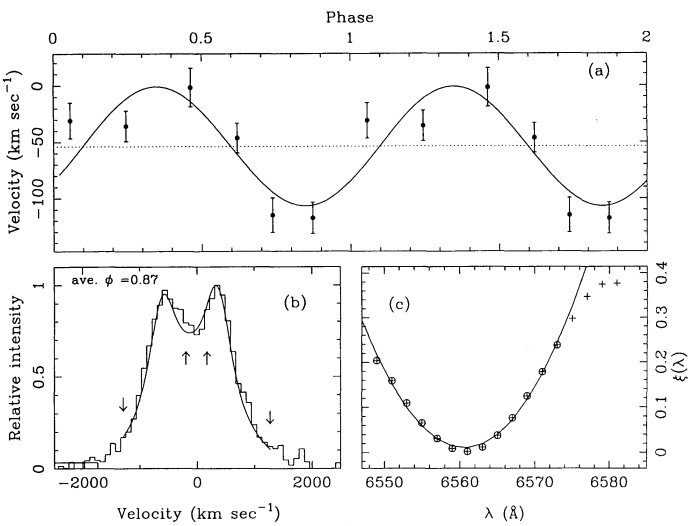

FIG. 5.—Same as Fig. 4, except that the results for the 1993 Nova Muscae data (both nights) are shown. See Table 6 for the sine curve parameters. The upward pointing arrows in panel (*b*) indicate the location of the five bins near the line core that were excluded from the fit.

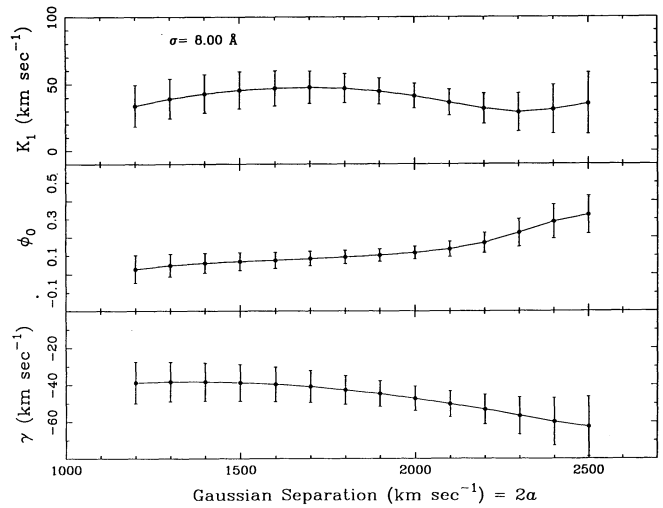

FIG. 6.—The diagnostic diagram for the 1993 Nova Muscae data, using $\sigma = 8.0$ Å. All three curves are relatively flat, which means that the sine curve parameters are not much different than the parameters with the lowest formal errors. The best-fitting sine curve occurs when $2a = 2000$ km s^{-1}.

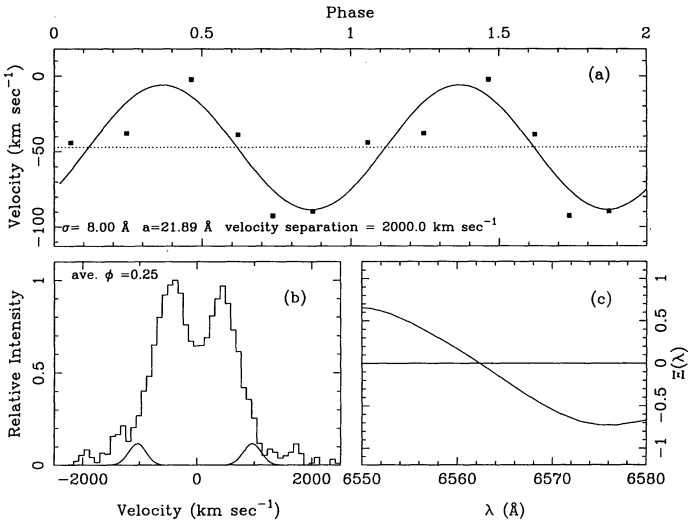

FIG. 7.—(*a*) The radial velocity curve for the Nova Muscae bins found using the double Gaussian method, with each point plotted twice for clarity. The Gaussian parameters are $\sigma = 8.0$ Å, and $2a = 2000$ km s^{-1}. See Table 7 for the sine curve parameters. (*b*) The profile with an average phase of $\phi = 0.25$ and the position of the double Gaussian (the negative Gaussian has been inverted). The midpoint between the two Gaussians is the centroid of the line. (*c*) The convolution function $\Xi(\lambda)$ for $\phi = 0.25$. The midpoint between the two Gaussians is defined to be the zero of $\Xi(\lambda)$.

$K_1 = 53 \pm 7.4$ km s^{-1}, larger than that of A0620−00, and $\phi_0 = 0.10 \pm 0.016$ (about 36°), which is once again inconsistent with the value of zero predicted if the emission-line velocities reflect the velocity of the primary object.

5.2. *Measuring Velocities by the Double Gaussian Technique*

We also measured the velocity curves of both Nova Muscae and A06200−00 using a technique developed by Schneider & Young (1980). This technique was used by HS90 in their study of the A0620−00 emission-line radial velocities. In this method the data are convolved with two identical Gaussian bandpasses. When the counts in each bandpass are equal, the midpoint between the two Gaussians is the wavelength of the spectral line (see Shafter 1985 for details). Note that this method assumes that the observed line profile is symmetric.

In general, the derived orbital parameters depend strongly on the half-separation (a) between the two Gaussians and weakly on the Gaussian width (σ). To assess the dependence of the sinusoid parameters on a, it is customary to plot them as a function of a in a "diagnostic diagram" (Shafter 1983; Shafter 1985; and Shafter, Szkody, & Thorstensen 1986). Examining these diagrams leads to a separation value that is wide enough to avoid hot spot contamination yet not so wide as to be dominated by noise from the continuum. This method will lead to an accurate velocity determination if the hot spot emission is confined to the outer regions of the disk so that its contribution to the line profile is confined to the low-velocity regions, as our models described in § 4.1 suggest. However, other sources of asymmetry, such as the excess blue emission we observe in some data sets, may invalidate the results.

Figure 6 shows the diagnostic diagram for the 1993 Nova Muscae data, using $\sigma = 8.0$ Å. The $K_1(a)$, $\phi_0(a)$, and $\gamma(a)$ curves are relatively flat, and the fluctuation in the error bar sizes is small. Once again, $\phi_0(a) > 0$ for most values of a. Thus the phase shift noted in the previous section is present in the velocity curve constructed with a quite different method.

The smallest errors in Figure 6 occur for $2a = 2000$ km s^{-1}. Table 7 lists the sine curve parameters, and Figure 7*a* shows the radial velocity curve. Figure 7*b* shows the position of the double Gaussian at phase $\phi = 0.25$. The Gaussian separation is wide enough to avoid major contamination from the peaks, and small enough to avoid the noise in the extreme line wings. Separations greater than 2000 km s^{-1} are affected by the noise in the extreme line wings, and the errors shown in Figure 6 do indeed rise past $2a = 2000$ km s^{-1}. The best-fitting value of $K_1 = 41.4 \pm 9.3$ km s^{-1} for Nova Muscae found using the double Gaussian technique agrees within the errors with the value of $K_1 = 53.0 \pm 7.4$ found in § 5.1 using the model profile fitting.

As discussed above, the double Gaussian method works only for symmetric line profiles. Given the excess emission in

TABLE 7

BEST-FITTING SINE CURVE PARAMETERS FOUND USING DOUBLE GAUSSIAN TECHNIQUE (§ 5.2)

$2a$ (km s^{-1})	σ (Å)	K_1 (km s^{-1})	ϕ_0	γ (km s^{-1})	Comment
2100	5.5	12.9 ± 1.1	0.24 ± 0.015	1.5 ± 0.8	Best fit A0620−00
2100	4.0	10.6 ± 1.2	0.27 ± 0.020	0.9 ± 0.9	A0620−00
1800	5.5	25.2 ± 5.8	0.15 ± 0.037	−11.8 ± 4.1	A0620−00
2400	5.5	22.7 ± 4.7	0.18 ± 0.034	24.9 ± 3.4	A0620−00
1800	5.5	43.0 ± 8.0	0.16 ± 0.031	−28.0 ± 6.0	HS90 A0620−00
2000	8.0	41.4 ± 9.3	0.12 ± 0.034	−47.2 ± 6.6	Best fit Nova Muscae

the blue wing of the A0620−00 line profiles, we do not expect the results of this method to reflect the motion of the primary. If one nevertheless attempts to use the double Gaussian method on these data, one obtains a low value of the velocity semiamplitude K_1 (12.1 ± 1.1 km s^{-1}), consistent with what one would expect of the excess blue emission were approximately stationary in velocity space. Curiously, despite the presence of excess blue emission in their data, HS90 find a velocity semiamplitude of $K_1 = 43 \pm 8$ km s^{-1} using the double Gaussian method (see Table 7). This result suggests that the excess blue emission seen in their data does vary with phase, and is different from what we see in the data reported here.

5.3. *Calculation of the Mass Ratio*

Taking the values of K_1 computed in § 5.1 (see Table 6) as a measure of the motions of the primaries, we can determine the mass ratios of Nova Muscae and A0620−00 by comparing the measurements of K_1 with the corresponding values of K_2 listed in Table 8. *However, since the emission line radial velocity curves are phase-shifted (i.e., $\phi_0 \neq 0$), the observed emission-line radial velocity curve cannot accurately represent the true radial velocity of the primary.* It is possible that the observed K_1 is related to the true velocity semiamplitude of the primary, but the nature of this relation is unknown. The phase zero points of both Nova Muscae and A0620−00 are firmly established since the secondary velocity curves on which the zero points are based came in part from the same data that we discuss here. Thus errors in phasing between the primary and secondary light curves cannot account for the observed phase shift in either source. A second source of possible error that can be ruled out is hot spot contamination. We do observe weak hot spot activity in A0620−00 and Nova Muscae (Fig. 3), but the hot spot is in phase with the secondary star in both cases ($\psi_{hs} \approx 0°$, see Table 5). The hot spot contamination might lower $K_1(a)$ for small a (HS90), but it cannot shift the phase zero-point of the radial velocity curve. Also, the phase shifts found using the double Gaussian technique were nonzero at most separations in both cases, and the value of $\phi_0(a)$ generally increases as the separation $2a$ increases, which is the opposite of what is expected from the hot spot contamination confined to the outer parts of the disk.

If we take the measurements of K_1 for A0620−00 and Nova Muscae at face value, then the implied mass ratio q of A0620−00 is 0.074 ± 0.006 (i.e., $M_1 \approx 14M_2$). MRW94 found $q = 0.067 \pm 0.01$ ($M_1 \approx 15M_2$) from their study of the rotational broadening of the absorption lines from the mass donor. Haswell et al. (1993) found that $q \gtrsim 0.094$ ($M_1 \lesssim 10.6M_2$) from their A0620−00 light curve models, and HS90 found $q = 0.094 \pm 0.018$ using the double Gaussian technique (see Table 9). The A0620−00 mass ratio found in the present work is thus in good agreement with MRW94's previous result, and in reasonable agreement with the results of HS90 and Haswell et al. (1993), *despite the presence of the large phase shift in the emission-line radial velocity curve.* It would be of great interest for further determinations of K_1 and ϕ_0 via model profile fitting to test how repeatable these parameters are. For Nova Muscae, the implied mass ratio using the value of K_1 found in § 5.1 is $q = 0.133 \pm 0.019$, or $M_1 \approx 8M_2$ (see Table 9). Antokhina & Cherepashchuk (1993) found $12M_2 \leq M_1 \leq 21M_2$ from their model of the I-band light curve of Nova Muscae given in Remillard et al. (1992). We finally note that all of these values for q are inconsistent with the limits derived from interpretation of the 1991 A0620−00 and Nova Muscae Hα emission-line profiles (§ 3.2).

TABLE 9

MEASUREMENTS OF THE MASS RATIO FOR A0620−00 AND NOVA MUSCAE

System	Mass Ratio ($q = M_2/M_1$)	Reference
A0620−00	0.067 ± 0.010	MRW94
A0620−00	0.094 ± 0.018	HS90
A0620−00	>0.094	Haswell et al. 1993
A0620−00	0.074 ± 0.006	This work
Nova Muscae	0.0476 − 0.0833	Antokhina & Cherepashchuk 1993
Nova Muscae	0.133 ± 0.019	This work

6. ASYMMETRY IN THE EMISSION-LINE WINGS

The simple emission-line models we have discussed with and without hot spots predict profiles that are symmetric in the line wings. However, as we have seen, not all of the observed line profiles are symmetric. Figure 8 shows the residuals (data-model) for summed Hα emission-line profiles from Nova Muscae in 1992 and 1993, and from A0620−00 on both nights in 1991. To see how the excess blueshifted emission components depend on phase, we computed the residuals of the six phase-resolved 1992 Nova Muscae profiles and the 10 1991 A0620−00 profiles shown in Figure 3. To describe the phase dependence of the strength of the excess emission quantitatively, we define the following quantity:

$$\mathscr{S} \equiv \frac{\sum_{\text{low bin}}^{\text{high bin}} p \times [f(\Lambda_i) - F(u_{\Lambda_i})]}{\sum_{\text{profile}} p \times F(u_{\Lambda_i})}, \quad (5)$$

where $f(\Lambda_i)$ is the y-value of the data at wavelength Λ_i (where the peak y-value is unity), $F(u_{\Lambda_i})$ is the height of the model (eq. [3]) at the radial velocity corresponding to the wavelength Λ_i, and p is the pixel size. The quantity $\mathscr{S}$ represents the area of the residuals, normalized to the area under the entire model profile. The model $F(u_{\Lambda_i})$ is defined by the parameters listed in

TABLE 8

ORBITAL PARAMETERS FOR A0620−00 AND NOVA MUSCAE

Parameter	Result for A0620−00	Result for Nova Muscae
Orbital period (days)	0.323014 ± 0.000001	0.43325 ± 0.00058
K velocity (km s^{-1})	443 ± 4	399.3 ± 8.0
γ velocity (km s^{-1})	10 ± 5	1.0 ± 5.7
T_0 (spectroscopic) (HJD 2,440,000+)	$6{,}082.7488 \pm 0.0002$	$9{,}045.7744 \pm 0.0012$
Mass function ($M_\odot$)	2.91 ± 0.08	2.86 ± 0.17

NOTE.—These results incorporate recent unpublished data.

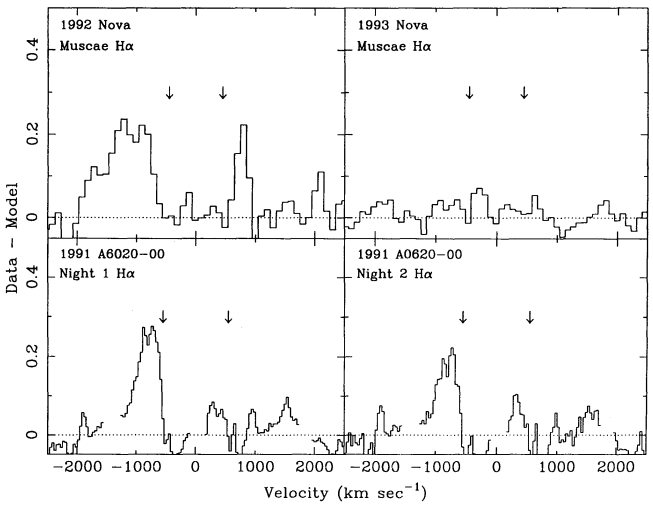

FIG. 8.—The residuals (data minus model) for four composite profiles are shown. The x-axis is in velocity units, and the y-axis units are normalized such that the peak heights of the profiles are unity. Arrows point to the velocity coordinates of the profile peaks. Upper left plot shows the residuals of the 1992 Nova Muscae profile shown in Fig. 1, while upper right plot shows the 1993 Nova Muscae residuals. 1991 Night 1 A0620−00 data (*lower left*) was averaged separately from Night 2 data (*lower right*).

Table 5. We defined the upper bin numbers to be the bin where the data on the blue wing of the profiles in Figure 1 first deviates significantly from the model fits. For Nova Muscae, the velocity of this point is $v \approx -600$ km s^{-1}, and for A0620−00 $v \approx -550$ km s^{-1}. The quantity $\mathscr{S}$ as a function of phase is plotted in Figure 9 for Nova Muscae and A0620−00 (Night 1). The shape of the Night 1 A0620−00 $\mathscr{S}(\phi)$ curve is remarkably similar to the 1992 Nova Muscae $\mathscr{S}(\phi)$ curve, although the total amount of the emission is different.

The changes between 1992 and 1993 in Nova Muscae show that the excess blue emission is transient over a timescale of $\lesssim 10$ months, so the mechanism responsible for it must vary on these timescales. The emission might be due to an outflow from the accretion disk (HS90) or from the system as a whole, in which case the redshifted emission would have to be hidden, perhaps by the accretion disk (although we note that there is a narrow redshifted component in the 1992 Nova Muscae residuals). Since the emission is seen at all orbital phases a jetlike structure is implausible.

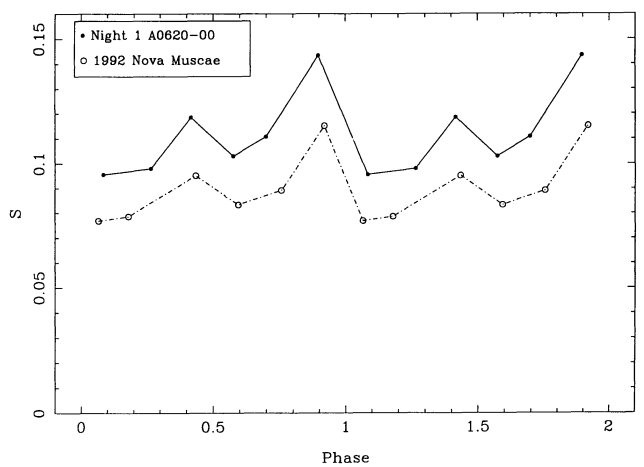

FIG. 9.—The quantity $\mathscr{S}$ which represents the area of the blueshifted emission component normalized to the area under the model profile (eq. [5]) is shown as a function of phase for the 1992 Nova Muscae and 1991 Night 1 A0620−00 residuals (data-model). Each point has been plotted twice for clarity. Night 2 A0620−00 data are not plotted due to incomplete phase coverage.

7. CHANGES IN THE EQUIVALENT WIDTHS OF THE BALMER LINES

The equivalent widths (EWs) of the Hα lines vary in both Nova Muscae and A0620−00. To measure the EWs of the Hα lines in the A0620−00 spectra (disk + secondary star), we integrated pixel intensities between bad data regions in the extreme line wings. Figure 10 shows the Hα EWs for A0620−00 as a function of phase. There is clear evidence for periodic modulation in the Night 1 Hα EWs as a function of phase, with the maximum EW at phases $\phi = 0.0$ and 0.5 (the conjunction phases) and the minimum EW at phases $\phi = 0.25$ and 0.75 (the quadrature phases). The data of MRW94, based on observations taken at the beginning of 1992, show a similar dependence of the A0620−00 Hα EW on phase. The Night 2 Hα EWs also show some evidence for periodic variation, but the phase coverage is incomplete and the quality of the data is much lower. The EWs of the Hα lines in the 1993 data are significantly lower than the 1991 EWs.

MRW94 suggested that the EW modulation was due to the changing continuum flux from the secondary over the orbit (ellipsoidal variations). We have attempted to model the EW variation in A0620−00 on the assumption that the EW modulation is a result of the ellipsoidal variations of the secondary star. The solid curve in Figure 10 is a model light curve for reasonable parameters for this system calculated using a program written by Yoram Avni (1978, see also McClintock & Remillard 1990). Since the phase of minimum flux from the secondary would correspond to the maximum EW from the system, the model light curve was inverted (so that the maxima are of unequal heights) and superposed on the data shown in Figure 10. No attempt to measure the goodness of fit was made. Given the potential for large systematic errors caused by

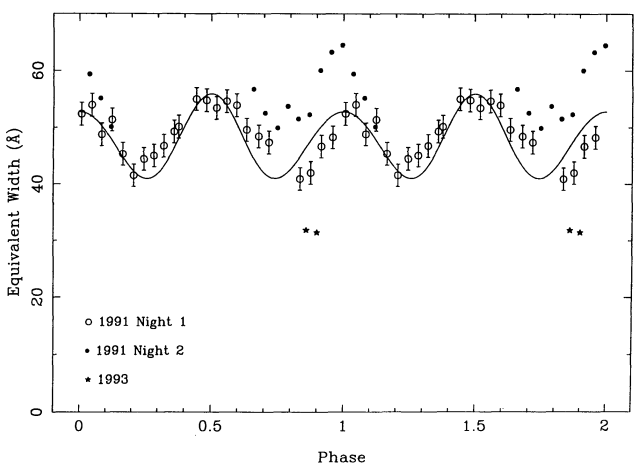

FIG. 10.—Equivalent widths of the Hα lines in the A0620−00 data as a function of phase. 1991 Night 1 data are shown with the open circles, 1991 Night 2 data are shown with the filled circles, and 1993 data are shown with the filled stars. Each point is plotted twice for clarity. Error bars shown with Night 1 data reflect the estimated uncertainty in the equivalent widths caused by the bad data regions in the extreme line wings only. The error caused by the bad data region at the center of the profile was not estimated. The solid line is a light curve model described in the text, using an inclination of $i = 70°$ and a mass ratio of $1/q = 13$. The curve was scaled by eye, and no attempt was made to find the best-fit light curve parameters.

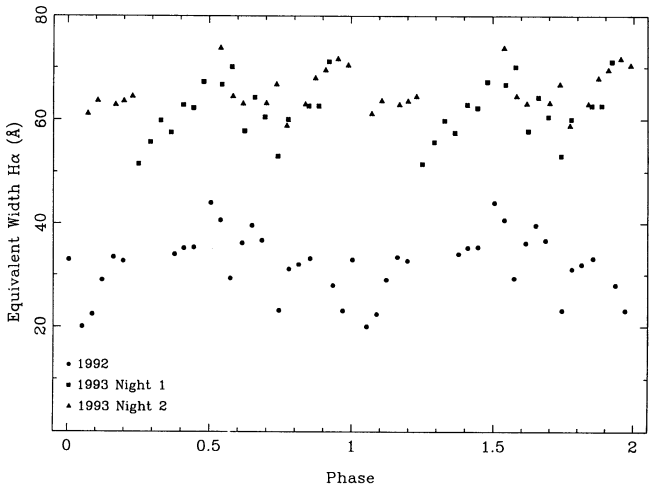

FIG. 11.—Equivalent widths of the Hα lines in the Nova Muscae data as a function of phase. 1992 data are shown with the filled circles, data from the first night of the 1993 data are shown with the filled squares, and data from the second night of the 1993 data are shown as the filled triangles. Each point has been plotted twice for clarity.

the bad data regions, the fit of the Night 1 EW data to the model curve is surprisingly good. Better spectroscopic observations and simultaneous photometric observations covering several orbital cycles will be needed to see if the shape of the EW curve is in fact well fitted by an ellipsoidal light curve model.

The Hα EWs of the Nova Muscae data are shown as a function of phase in Figure 11. The 1993 EWs show a trend similar to the trend in the 1991 Night 1 A0620−00 EWs, but the scatter is larger. The 1992 Nova Muscae EW curve does not seem to show the same trend as the 1993 EW curve. It is clear from Figure 11 that the EWs of the Hα lines in the 1993 data are about a factor of 2 bigger than the EWs of the lines in the 1992 data. The Hβ EW's show a similar overall increase from 1992 to 1993. A possible explanation for the change in EW from year to year is a difference in the continuum emission from the system. Since it is unlikely that the luminosity of the secondary star would decrease dramatically within a period of 10 months, the change must be in the disk continuum. We therefore suggest that the accretion disk was still in the process of returning to its quiescent state during the 1992 observations, which were only 15 months after the outburst. However, we cannot rule out an *increase* in the actual Hα and Hβ flux between the two observing runs.

8. DISCUSSION

Modeling the emission lines in quiescent black hole binary systems can, in principle, reveal important information about these systems. Our data show that simple Keplerian, optically thin α-disk models often provide a good fit to the averaged emission-line profiles. However, the physical interpretation of these models must be more complex than is at first apparent, for upon closer inspection several difficulties arise with the straightforward interpretation of the models. The optically thin symmetric models which fit the phase-averaged profiles do not fit the phase-resolved spectra which reveal the existence of time variable hot spots and regions of optical thickness. The occasional presence of excess blue emission (of unknown origin) can invalidate emission-line velocity curves constructed using the Schneider & Yong (1980) method. Constructing velocity curves using only information from the red side of the profile (as we do in § 5.1) may be more reliable, but the curious phase shift persists, casting doubt on what is really being measured. Finally, the unreasonably low values of the mass ratio inferred from the velocity of the outer edge of the disk suggest that the assumption of Keplerian motion, on which the entire modeling effort is based, may be flawed. Thus models which appear at first glance to fit the data very nicely display details which call their validity into question. Nevertheless, these models provide a valuable parameterization of the data.

The value of this parameterization is highlighted by the remarkable similarities between the two sources. These similarities confirm the fact that the difficulties in interpretation do not arise as the result of random errors in the data collection. They also add to the list of characteristics of black hole X-ray novae (BHXNs). Specifically, both A0620−00 and Nova Muscae display the following.

1. Phase-averaged Balmer emission lines which are well fitted by optically thin Keplerian disk models with $\alpha = 1.5$.
2. Excess emission superposed on the blue wing of the emission lines which varies on a timescale of months from 0 to ~10% of the total emission. When the excess emission is present its strength and position in velocity space are fairly constant as functions of orbital phase (with possible slight increases in the strength at phases $\phi = 0.4$ and $\phi = 0.9$). The presence of this blue emission can create systematic errors in determining the velocity centroid of the emission lines.
3. Ratios of the implied velocity of the outer edge of the disk to that of the secondary star which are remarkably low, in the range 1.1–1.2. Even with the assumption that the disk extends to the outermost closed streamline, this result implies unreasonably low mass ratios. The most likely resolution of this difficulty is that the assumption of Keplerian motion needs to be abandoned near the edge of the disk.
4. Evidence for a broad relatively low surface brightness hot spot which appears when the emission lines are binned in phase. The surface brightness excess is characterized by a value of the parameter β which varies on timescales of months to years from 0.05 to 0.15. Regions of optical thickness in the disk are also indicated, and stochastic variability is required to account for the remaining differences between the models and the data.
5. Velocity variations of the central wavelengths of the Hα emission lines which are seen over an orbital cycle. These variations seem to imply mass ratios $q \lesssim 0.1$. However, in both systems the phase of the emission line variability is $\approx 140°$ away from that of the velocity curve of the secondary star—if the motion truly represented motion of the primary, the phase shift would be 180°.

These phenomena are not all unique to Nova Muscae and A0620−00. For example, Casares and Charles (1992) found that the Hα emission line in the long-period black hole binary V404 Cyg had an additional blue component (in addition to a broad component for the base and two Gaussians for the peaks). Marsh, Horne, & Shipman (1987) found that the blueshifted peaks in the emission lines of the dwarf nova Z Chamaeleontis were consistently stronger than their redshifted counterparts, and that this asymmetry persisted through the binary orbit. Phase shifts are also seen in a subclass of CVs known as SW Sex stars (Thorstensen, Davis, & Ringwald 1991). Some of these systems eclipse, and the Hα emission-line radial velocity curves lag in phase with respect to the eclipse.

There are significant changes in the emission lines between our two sets of observations of Nova Muscae and between our observations of A0620−00 and those of previous workers. These changes may indicate changes in the disks, which might potentially be used to constrain models of the disk outburst cycle (Osaki, Hirose, & Ichikawa 1993 and references therein). We can point to four different changes in the Nova Muscae system, which are generally model-independent. First, the 1992 Hα emission-line profile is asymmetric in its line wings, and the 1993 Hα emission-line profile is not. Second, the depths of the central minima are not constant with phase, this can be seen in Figure 3. It was shown in § 4.2 that emission from an optically thick disk can account for the deep central minima, which suggests that (within the context of our model) the large regions of optical thickness have moved around the disk (with respect to the secondary star which defines the orbital phase). Third, the peak heights in the 1992 phase-resolved Nova Muscae profiles vary by a larger amount than they do in the 1993 profiles (Fig. 3). The model-dependent explanation for this is the hot spot amplitude β has decreased by a factor of 3. Finally, the equivalent widths of the Balmer lines in the 1993 spectra are a factor of 2 *larger* than they were in the 1992 data (Fig. 11). This may be due to a change in the continuum emission from the disk or to higher flux in the Balmer lines. Clearly, the shape of the Hα emission line profile has changed between 1992 April and 1993 February, but it is unclear how much, if any, the Hα flux has changed.

We can point to two significant changes in our A0620−00 data that are model-independent. First, the peaks in the 1993 Hα profile have a larger separation than they did in 1991. The corresponding increase in the disk velocity v_d is 100 km s^{-1}. The larger disk velocity in 1993 suggests that the disk has contracted between 1991 and 1993. Second, the 1993 Hα emission line profile is symmetric in its line wings, and the 1991 profiles are not. Comparing our observations of A0620−00 to those of JKO89, we note that the summed emission-line profile shown in Figure 4 of JKO89 (based on observations from 1986 March) is symmetric in the line wings, unlike the profile shown in Figure 1. The summed Hα profile shown in Figure 2 of HS90 (based on observations made 1989 December and 1990 January) is asymmetric in the line wings. There appears to be an extra blueshifted emission component similar to the one observed in our data (Fig. 8). Since HS90 used a different emission-line model, we cannot easily compare results. Finally, the Doppler images of the A0620−00 accretion disk shown in MRW94 (based on observations from 1991 December and 1992 January) have excess emission in the region of velocity space which corresponds to excess blue emission in the Hα line profile. Thus the extra blueshifted emission component was absent in early 1986, appeared between 1986 and 1990, and disappeared between early 1992 and late 1993.

9. SUMMARY

The conclusions of this paper can be summarized in three basic points.

1. Standard α-disk models, augmented by hot spots and regions of optical thickness, appear to provide an excellent fit to the Hα emission lines of A0620−00 and Nova Muscae in quiescence. The only significant deviation from these models appears to be a time-variable excess in the blue wing of the line.

2. A number of difficulties arise in providing a consistent physical interpretation of the models. In particular, the large phase offsets of the emission-line radial velocity curves call into question the association of the emission-line radial velocities with the primary radial velocity variations. The small ratios of the disk velocity to the secondary star velocity seem to indicate that the assumption of Keplerian velocities near the outer disk edge is not completely valid. We conclude that while these models are useful parameterizations of the emission lines, the physical conditions of the accretion disks which give rise to these emission lines are complex and not yet fully understood.

3. These two sources have notably similar emission line profiles. In particular, both sources have (*a*) identical accretion disk radial emissivity distributions [$f(r) \propto r^{-1.5}$]; (*b*) regions on the disk with increased emission (hot spots); (*c*) similar variations in the strength of the excess blue emission (when present); (*d*) emission-line radial velocity curves with comparable amplitudes and phase offsets; (*e*) values of the ratio of the disk velocity to the secondary star velocity which imply small mass ratios.

These characteristics may prove to be a new diagnostic of black hole systems.

We thank the helpful staff at CTIO for their excellent support. We would also like to thank J. DeVeny and K. Loken for their help at Kitt Peak. C. B. F. gratefully acknowledges the support from the NSF grant AST 90-01181. Partial support was also provided by the NSF grant AST 86-12572 and the NASA grant NAGW-2469.

REFERENCES

Antokhina, É. A., & Cherepashchuk, A. M. 1993, Astron. Lett., 19, 3
Avni, Y. 1978, in Physics and Astrophysics of Neutron Stars and Black Holes, ed. R. Giacconi & R. Ruffini (Amsterdam: North-Holland), 42
Bailyn, C. D. 1992, ApJ, 391, 298
Casares, J., & Charles, P. A. 1992, MNRAS, 255, 7
Casares, J., Charles, P. A., & Naylor, T. 1992, Nature, 355, 614
Charles, P. A., et al. 1991, MNRAS, 249, 567
Chitre, D. M., & Hartle, J. B. 1976, ApJ, 207, 592
Della Valle, M., Jarvis, B. J., & West, R. M. 1991, Nature, 353, 50
Filippenko, A. V. 1982, PASP, 94, 715
Filippenko, A. V., Romani, R. W., Sargent, W. L. W., & Blandford, R. D. 1988, AJ, 96, 242
Haswell, C. A., Robinson, E. L., Horne, K., Stiening, R. F., & Abbott, T. M. 1993, ApJ, 411, 802
Haswell, C. A., & Shafter, A. W. 1990, ApJ, 359, L47 (HS90)
Horne, K. 1994, in Proc. NATO Advanced Research Workshop Theory of Accretion Disks 2, eds. W. Duschl, J. Frank, F. Meyer, E. Meyer-Hofmeister, & W. Tscharnuter (Dordrecht: Kluwer)
Horne, K., & Marsh, T. R. 1986a, MNRAS, 218, 761
———. 1986b, in The Physics of Accretion onto Compact Objects (Lecture Notes in Physics, 266), ed. H. Arake et al. (New York: Springer), 1
Johnston, H. M., Kulkarni, S. R., & Oke, J. B. 1989, ApJ, 345, 492 (JKO89)
Kitamoto, S., Tsunemi, H., Miyamoto, S., & Hayashida, K. 1992, ApJ, 394, 609
Marsh, T. R., Horne, K., & Shipman, H. L. 1987, MNRAS, 225, 551
Marsh, T. R., Robinson, E. L., & Wood, J. H. 1994, MNRAS, 266, 137 (MRW94)
McClintock, J. E., & Remillard, R. A. 1986, ApJ, 308, 110
———. 1990, ApJ, 350, 386
Osaki, Y., Hirose, M., & Ichikawa, S. 1993, in Accretion Disks in Compact Stellar Systems, ed. J. C. S. Wheeler (Singapore: World Scientific), 1
Paczyński, B. 1977, ApJ, 216, 822
Remillard, R. A., McClintock, J. E., & Bailyn, C. D. 1992, ApJ, 399, L145
Rhoades, C. E., & Ruffini, R. 1974, Phys. Rev. Lett., 32, 324
Schneider, D. P., & Young, P. 1980, ApJ, 238, 946
Shafter, A. W. 1983, ApJ, 267, 222
———. 1985, in Cataclysmic Variables and Low-Mass X-Ray Binaries, ed. D. Q. Lamb & J. Patterson (Dordrecht: Reidel), 355
Shafter, A. W., Szkody, P., & Thorstensen, J. R. 1986, ApJ, 308, 765
Shakura, N. I., & Sunyaev, R. A. 1973, A&A, 24, 337
Shapiro, S., & Teukolsky, S. 1983, Black Holes, White Dwarfs, and Neutron Stars (New York: Wiley)
Smak, J. 1981, Acta Astron., 31, 395
Thorstensen, J. R., Davis, M. K., & Ringwald, F. A. 1991, AJ, 102, 683